Hindawi
Advances in Civil Engineering
Volume 2019, Article ID 7831656, 7 pages
https://doi.org/10.1155/2019/7831656

Research Article

An Improved Statistical Damage Constitutive Model for Granite under Impact Loading

Zhenwei Zhao,[1,2] Bo Wu,[3] Xin Yang,[1,4] Zhenya Zhang,[5] and Zhantao Li[5]

[1]*School of Civil Engineering, Fujian University of Technology, Fuzhou 350118, China*
[2]*Fujian Provincial Key Laboratory of Advanced Technology and Informatization in Civil Engineering, Fuzhou 350118, China*
[3]*College of Civil Engineering and Architecture, Guangxi University, Nanning 530004, China*
[4]*Key Laboratory of Underground Engineering, Fujian University of Technology, Fuzhou 350118, China*
[5]*School of Architecture and Transportation Engineering, Ningbo University of Technology, Ningbo 315211, China*

Correspondence should be addressed to Bo Wu; wubo@gxu.edu.cn

Received 29 April 2019; Revised 28 June 2019; Accepted 30 July 2019; Published 14 August 2019

Academic Editor: Mostafa Sharifzadeh

To study the impact properties of granite, the parameters (including the stress-strain curve, elasticity modulus, peak strength, and peak strain) of the test pieces in each group were determined via standard split-Hopkinson pressure bar tests. The results revealed that the prepeak stress-strain curves are approximately linear; the postpeak stress-strain curve declined sharply and exhibited the characteristics of brittle material failure after the stress exceeded the peak strength. In terms of the specimen form following failure, for increasing strain rate, the granite specimen became increasingly fragmented after failure. In addition, the single-parameter statistical damage constitutive model was improved, and a double-parameter statistical damage constitutive model for describing the total stress-strain curve of granite under the action of impact loading was proposed. The parameters of the statistical damage model, m and a, were obtained via fitting. The results revealed that the parameter m decreases with increasing elasticity modulus, whereas the parameter a increases. Similarly, the peak strength and the peak strain increased (in general) with increasing strain rate.

1. Introduction

In many practical engineering problems, the applied load is dynamic. For example, rock blasting and excavation involve mechanical properties associated with the dynamic failure of rocks. The mechanical characteristics of impact have been extensively investigated. Vostretsov and Yakovitskaya [1] studied the mechanical properties of a preloaded rock specimen under the action of an impact load. Li et al. [2] proposed a novel technique for combined dynamic and static loading of a rock. The results revealed that, for this type of loading, the strength of the rock decreased significantly when the axial preload exceeds 70% of the static load strength of the rock. Wang et al. [3] studied the nonlinear damage of brittle rock under the action of an impact load. Furthermore, Millon et al. [4] investigated the mechanical characteristics of sedimentary rocks under the action of an impact load and the fragmentation of rock under different strain rates. Wu et al. [5] proposed a method for quantifying the fatigue damage of brittle rocks under an impact load. Peng et al. [6] assessed the failure process and the governing mechanism in sandstone under biaxial isostatic pressure and found that microcrack propagation is more likely under a combined load than under separate loads. Through numerical simulation, Bi et al. [7] evaluated the failure process of the rock material under the action of an impact load. Saksala [8] used a viscoplastic damage model to investigate the low-frequency impact loading of rocks. Wang and Yang [9] studied the dynamic fracture toughness of coal rocks under the action of an impact load. Liu et al. [10] assessed the acoustic emission wavelet denoising threshold of rocks under a dynamic load. Scherbakov and Chmel [11]

investigated the impact fracture characteristics of granite at different temperatures. In addition, Wang et al. [12–14] and Meng et al. [15] studied the mechanical behavior of clayey soil under different conditions and the weakening mechanisms of gypsum interlayers from Yunying salt, respectively. Tu et al. [16] proposed a new criterion for defining slope failure.

Previous studies have shown that the mechanical behavior of rocks under an impact load differs significantly from that under a static load. However, theoretical analyses and experimental studies focused on the dynamic failure of rock materials are rare, and thus, the dynamic characteristics of rocks under impact loading have received an increasing attention. Therefore, in the present work, granite specimens are subjected to a split-Hopkinson pressure bar (SHPB) test. The model parameters of specimens in each group are obtained via fitting based on the improved statistical damage constitutive model. The determined impact properties of granite are important from both theoretical and practical points of view.

2. Tests

2.1. Testing Process. Cylindrical 63 mm × 31.5 mm black granite specimens with a diameter (D)-to-height (H) ratio of $D:H=2:1$ were tested. To guarantee the flatness of the upper and lower surfaces, these surfaces were symmetrically ground with a grinder. In the standard SHPB test, specimens with a diameter-to-height ratio of 2 were investigated (Figure 1). The SHPB consisted of three parts (Figure 2 for the loading device): bullets, incident bar, and transmission bar. When a bullet strikes the incident bar, an incident wave will form, then propagate to the specimen along the bar, and interact with the specimen, resulting in a reflected wave and a transmission wave. The three types of wave can be measured by the strain gauge on the bar and acquired by an oscilloscope via an electrical bridge and ultrahigh dynamic strainometer.

2.2. Test Signal. Figure 3 presents the waveform signal of specimen #6 during testing. The black line and the red line denote the incident bar signal and the transmission bar signal, respectively. Incident waves, reflected waves, and transmission waves are typical triangular waves. The waveform suggests that the dynamic impact loading is a linear mode of loading and unloading that occurs immediately after the failure strength is reached, consistent with the dynamic failure characteristics of brittle materials.

2.3. Test Result. Figure 4 presents the dependence of the dynamic compression strength on the time. As shown in the figure, the dynamic failure process of the rock lasts for several dozens of microseconds. The minimum and maximum strengths are 189 MPa and 280 MPa, respectively. Most specimens have compression strengths of 260 MPa, except for specimens #2, #13, and #19, which have a slightly lower strength of 190 MPa–200 MPa.

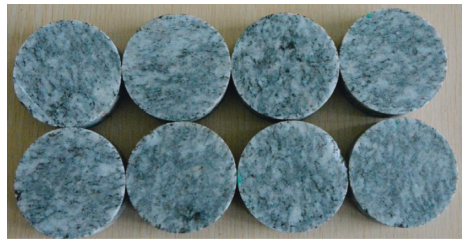

Figure 1: Partial specimens under dynamic compression (diameter-to-height ratio 2 : 1).

Figure 2: SHPB loading device.

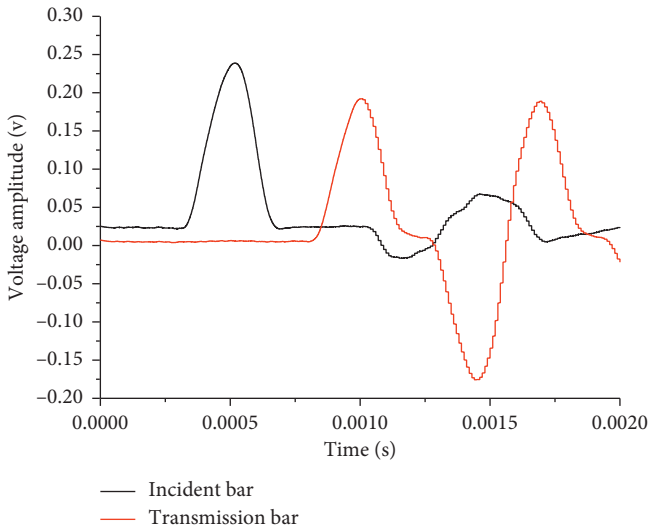

Figure 3: Signal diagram for specimen #6 under dynamic compression.

Figure 5 presents the stress-strain curve of dynamic compression. The prepeak stress-strain curves are approximately linear. However, the postpeak stress-strain curve declines rapidly after the stress exceeds the peak strength. An average dynamic compression strength of 240 MPa (average error: 18.75%) is determined. Most other failures occur at strain ranging from 7% to 9%, except in the case of specimen #8 where failure occurs at a strain of >11%, consistent with the failure characteristics of brittle materials. The fitted stress-strain curve is described by a linear elastic relationship, and an average dynamic modulus E_d of 31.5 GPa is determined.

Figure 6 shows the dependence of the dynamic compression strength on the strain rate ranging from 81

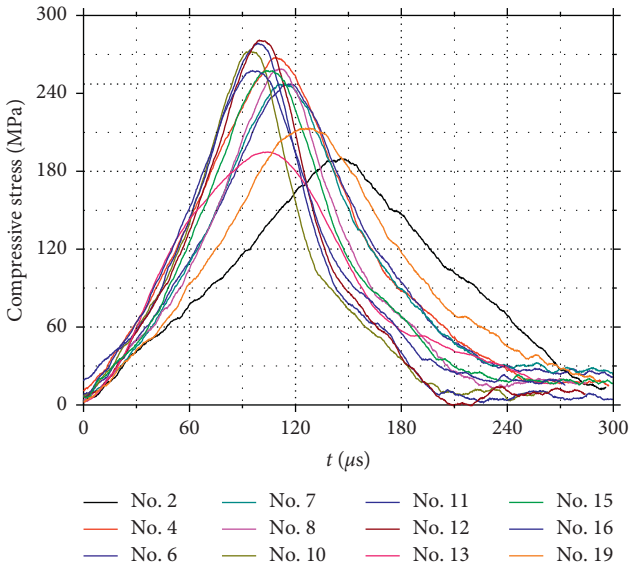

Figure 4: Dependence of the compression strength on time.

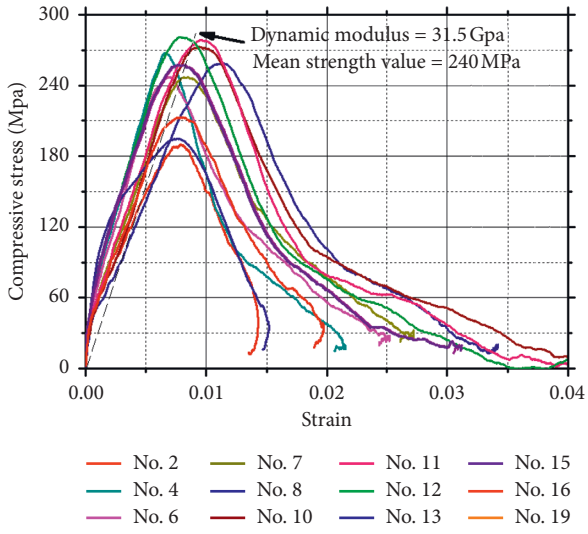

Figure 5: Dependence of the compressive stress on the strain.

to 210 s^{-1}. The strength increases significantly with increasing strain rate, indicating that the granite is hardened when withstanding the dynamic compression. Table 1 presents the test result of the granite under the action of the impact load.

2.4. Analysis of Failure Modes. The failure modes of some specimens are shown in Figure 7. Overall, the specimens are broken into pieces of different sizes under dynamic loading at different strain rates. The strain rates of specimens #2, #4, #6, #8, #13, and #19 are 81.90 s^{-1}, 81.26 s^{-1}, 107.02 s^{-1}, 185.98 s^{-1}, 97.34 s^{-1}, and 99.29 s^{-1}, respectively. With increasing strain rate, the fragment size and impact compressive strength of the granite specimens decrease and increase, respectively, after failure.

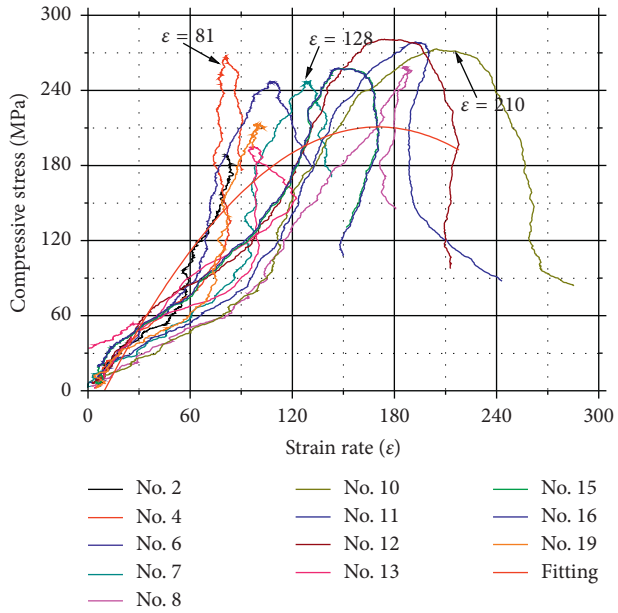

Figure 6: Dependence of the dynamic compression strength on the strain rate.

3. Improved Statistical Damage Constitutive Model of Granite under Impact Load

3.1. Improved Statistical Damage Constitutive Model. According to Krajcinovic and Silva [17], the Weibull distribution can be used to describe the internal damage of materials. Therefore, in this work, the microunit strength of granite is described by the Weibull distribution, with a probability density distribution function, which is given as

$$P(F) = \frac{m}{F_0}\left(\frac{F}{F_0}\right)^{m-1} \exp\left[-\left(\frac{F}{F_0}\right)^{m}\right], \quad (1)$$

where $P(F)$ and F are the probability density distribution function and strength distribution variable of the microunit, respectively, while m and F_0 are the Weibull distribution parameters.

The damage degree D can then be expressed as

$$D = \int_0^F P(y)dy = 1 - \exp\left[-\left(\frac{F}{F_0}\right)^{m}\right]. \quad (2)$$

The microunit strength based on the Drucker–Prager failure criteria is

$$F = \partial_0 \mathbf{I}_1 + \sqrt{\mathbf{J}_2},$$
$$\alpha_0 = \frac{\sin\varphi}{\sqrt{9 + 3\sin^2\varphi}}, \quad (3)$$

where φ is the internal frictional angle of the material, $\mathbf{I}_1$ is the first stress invariant of the stress tensor, and $\mathbf{J}_2$ is the second stress invariant of the stress tensor.

Li et al. [18] have reported that the microunit strength under a one-dimensional stress state is given as

Table 1: Test result of the granite under impact load.

Specimen number	Strain rate (s^{-1})	Elasticity modulus (GPa)	Peak strength (MPa)	Peak strain (%)
#2	81.90	37.90	189.95	0.784
#4	81.26	52.30	267.59	0.662
#6	107.02	49.64	246.99	0.686
#7	130.24	38.35	247.12	0.848
#8	185.98	29.19	253.03	1.016
#10	204.87	33.91	273.10	0.937
#11	192.40	38.81	278.51	0.955
#12	172.44	52.88	280.68	0.774
#13	97.34	89.78	194.71	0.758
#15	155.04	55.27	257.29	0.822
#16	153.87	57.73	257.23	0.809
#19	99.29	38.13	212.92	0.805

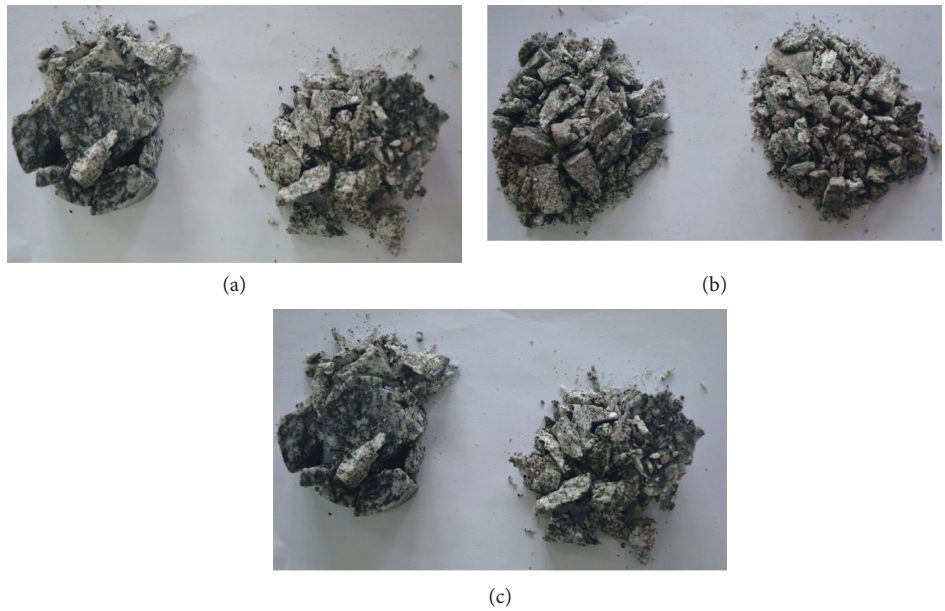

(a) (b) (c)

Figure 7: Photograph showing failure characteristics of (a) specimens #2 and #4, (b) specimens #6 and #8, and (c) specimens #13 and #19.

$$F = \left(\alpha_0 + \frac{1}{\sqrt{3}}\right) E\varepsilon_1, \tag{4}$$

where ε_1 is the axial strain.

The improved time-dependent damage models based on the Kelvin model include

$$\sigma = E\varepsilon_1 (1 - D) + \eta \frac{d\varepsilon_1}{dt}, \tag{5}$$

where σ, E, and η are the axial stress, elasticity modulus, and viscosity coefficient, respectively.

Substituting formula (2) into formula (5) gives

$$\sigma = E\varepsilon_1 \exp\left[-\left(\frac{F}{F_0}\right)^m\right] + \eta \frac{d\varepsilon_1}{dt}. \tag{6}$$

At the peak of the stress-strain curve $(\varepsilon_m, \sigma_m)$, $(d\varepsilon_1/dt) = 0$ and $(d\sigma/d\varepsilon_1) = 0$. Taking the derivative of formula (6) yields

$$F_0 = \left(\alpha_0 + \frac{1}{\sqrt{3}}\right) E\varepsilon_m m^{(1/m)}. \tag{7}$$

By substituting formula (7) into formula (6), we obtain

$$\eta \frac{d\varepsilon_1}{dt} = \sigma_m - E\varepsilon_m \exp\left(-\frac{1}{m}\right). \tag{8}$$

Substituting formulas (4) and (7) into formula (2) yields

$$D = 1 - \exp\left[-\frac{1}{m}\left(\frac{\varepsilon_1}{\varepsilon_m}\right)^m\right]. \tag{9}$$

The statistical damage computational formula, expressed as equation (9), consists of only one parameter, i.e., m. The prepeak damage and postpeak stress-strain curve slope are inadequately reflected by a single-parameter statistical damage constitutive model. In other words, the specimens with similar prepeak damage may have different postpeak stress-strain curve slopes, suggesting that the single-parameter statistical

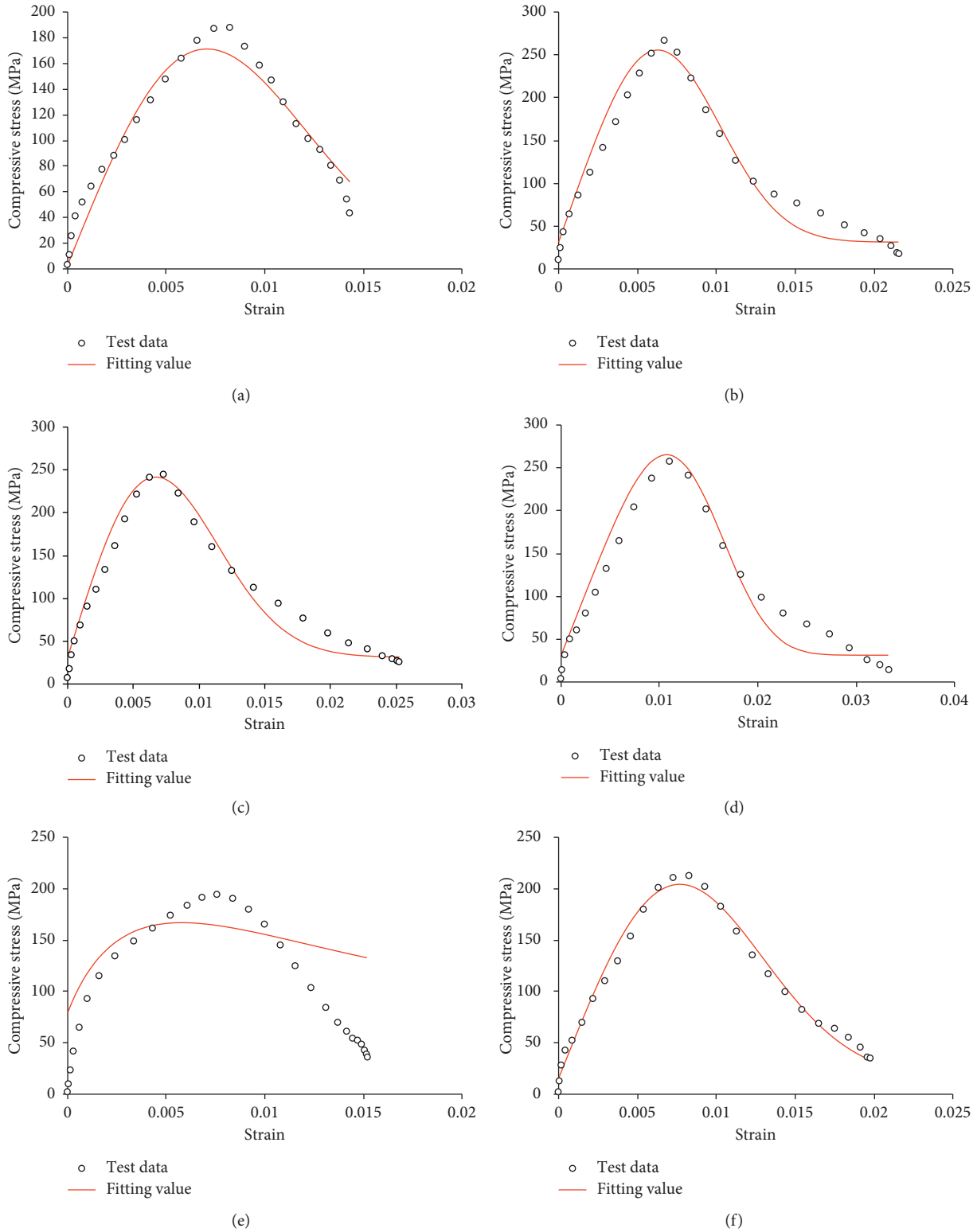

Figure 8: Comparison of the test data and the fitting result obtained for the statistical damage constitutive model: (a) specimen #2; (b) specimen #4; (c) specimen #6; (d) specimen #8; (e) specimen #13; (f) specimen #19.

damage constitutive model has limitations. For this reason, the present work proposes an improved computational formula for statistical damage:

$$D = 1 - \exp\left[-a\left(\frac{\varepsilon_1}{\varepsilon_m}\right)^m\right], \tag{10}$$

Table 2: Fitting result of the improved statistical damage constitutive model.

Specimen number	Strain rate (s^{-1})	m value	a value	Association coefficient R^2
#2	81.90	2.151	0.585	0.9536
#4	81.26	2.627	0.436	0.9666
#6	107.02	2.191	0.480	0.9625
#7	130.24	2.472	0.426	0.9637
#8	185.98	3.432	0.241	0.9501
#10	204.87	3.484	0.248	0.9390
#11	192.40	2.621	0.428	0.9706
#12	172.44	2.118	0.486	0.9768
#13	97.34	0.805	1.542	0.7391
#15	155.04	1.612	0.728	0.9823
#16	153.87	1.536	0.769	0.9791
#19	99.29	2.264	0.491	0.9850

where a and m are statistical damage parameters. Parameter a reflects the peak strength of the specimen; i.e., the peak strength of the specimen increases with decreasing a. The parameter m reflects the decline slope of the postpeak stress-strain curve; i.e., the decline slope of the curve increases with increasing m.

By substituting formulas (8) and (10) into formula (5), we obtain the expression describing the improved statistical damage constitutive model:

$$\sigma = E\varepsilon_1 \exp\left[-a\left(\frac{\varepsilon_1}{\varepsilon_m}\right)^m\right] + \sigma_m - E\varepsilon_m \exp\left(-\frac{1}{m}\right). \quad (11)$$

This formula describes the improved statistical damage constitutive model based on the Weibull distribution.

3.2. Fitting Result of the Improved Statistical Damage Constitutive Model. The fitting result of the improved statistical damage constitutive model is shown in Figure 8 and Table 2. As the table shows, good fitting results are obtained. A correlation coefficient of $R^2 > 0.9390$ is obtained for all specimens, except for specimen #13. The poor fitting result of this specimen results from the occurrence of significant plastic deformation and downward bending of the prepeak stress-strain curve, as shown in Figure 8(e). This trend differs significantly from the characteristics of other specimens, which are described by approximately linear prepeak curves. Based on Tables 1 and 2, parameter m decreases with increasing elasticity modulus, whereas parameter a increases. Similarly, the peak strength and the peak strain increase (in general) with increasing strain rate.

4. Conclusion

A statistical damage constitutive model is used to investigate the behavior of granite under impact loading. The major conclusions are summarized as follows:

(1) Under the impact load, the average dynamic modulus and average peak strength are 31.5 GPa and 240 MPa, respectively; the average peak strain ranges from 7% to 9%, consistent with the failure characteristics of brittle materials.

(2) The failure morphology of the granite samples indicates that, for increasing strain rate, the samples become increasingly fragmented after failure, and the impact compressive strength increases.

(3) The present work proposes an improved statistical damage constitutive model for granite subjected to an impact load and reveals the physical significance of the model parameters, m and a. The improved statistical damage constitutive model is used to fit the test data. A good fitting result is obtained, and the association coefficients are largely larger than 0.9390. Investigation of the parameters obtained via fitting revealed that parameter m decreases with increasing elasticity modulus, whereas parameter a increases. Similarly, the peak strength and the peak strain increase (in general) with increasing strain rate.

The impact behavior of rocks (including granite) is a complex scientific problem. In this work, the statistical damage theory is used to study this behavior from a macroscopic point of view and, hence, the present study has certain limitations. Therefore, future work will also consider the behavior from a microscopic point of view.

Data Availability

The data used to support the findings of this study are available from the corresponding author upon request.

Conflicts of Interest

The authors declare that they have no conflicts of interest.

Acknowledgments

This study was supported by the Fujian Provincial Natural Science Foundation Projects (grant no. 2018J01624), National Natural Science Foundation of China (grant nos. 51478118 and 51678164), Key Projects of Guangxi Natural Science Foundation (grant no. 2017JJD150035), Guangxi Science and Technology Base and Special Foundation For Talents (grant no. 2017AD23050), Open Fund of Key Laboratory of Underground Engineering (grant no. KFT18015), and Zhejiang Provincial Natural Science Foundation of China (grant no. LY16E040002). The authors gratefully acknowledge these supports.

References

[1] A. G. Vostretsov and G. E. Yakovitskaya, "Effect of external pulsed low-energy impact on destruction of pre-loaded rock specimens," *Journal of Mining Science*, vol. 50, no. 6, pp. 1033–1039, 2014.

[2] X. Li, Z. Zhou, T.-S. Lok, L. Hong, and T. Yin, "Innovative testing technique of rock subjected to coupled static and dynamic loads," *International Journal of Rock Mechanics and Mining Sciences*, vol. 45, no. 5, pp. 739–748, 2008.

[3] Y. X. Wang, P. Cao, Y. H. Huang, R. Chen, and J. T. Li, "Nonlinear damage and failure behavior of brittle rock subjected to impact loading," *International Journal of Nonlinear Sciences and Numerical Simulation*, vol. 13, no. 1, pp. 61–68, 2012.

[4] O. Millon, M. L. Ruiz-Ripoll, and T. Hoerth, "Analysis of the behavior of sedimentary rocks under impact loading," *Rock Mechanics and Rock Engineering*, vol. 49, no. 11, pp. 4257–4272, 2016.

[5] B. Wu, P. Kanopoulos, X. Luo, and K. Xia, "An experimental method to quantify the impact fatigue behavior of rocks," *Measurement Science and Technology*, vol. 25, no. 7, article 075002, 2014.

[6] J. Y. Peng, Y. H. Li, F. P. Zhang, and Z. G. Qiu, "Failure process and mechanism of sandstone under combined equal biaxial static compression and impact loading," *Strain*, vol. 54, no. 2, article e12267, 2018.

[7] J. Bi, X. P. Zhou, and X. M. Xu, "Numerical simulation of failure process of rock-like materials subjected to impact loads," *International Journal of Geomechanics*, vol. 17, no. 3, article 04016073, 2017.

[8] T. Saksala, "Damage-viscoplastic consistency model with a parabolic cap for rocks with brittle and ductile behavior under low-velocity impact loading," *International Journal for Numerical and Analytical Methods in Geomechanics*, vol. 34, no. 13, pp. 1362–1386, 2010.

[9] Y. Wang and R. Yang, "Study of the dynamic fracture characteristics of coal with a bedding structure based on the NSCB impact test," *Engineering Fracture Mechanics*, vol. 184, pp. 319–338, 2017.

[10] X.-L. Liu, Z. Liu, X.-B. Li, M. Rao, and L.-J. Dong, "Wavelet threshold de-noising of rock acoustic emission signals subjected to dynamic loads," *Journal of Geophysics and Engineering*, vol. 15, no. 4, pp. 1160–1170, 2018.

[11] I. P. Scherbakov and A. E. Chmel, "Impact fracture of granite at temperatures from 20 to 500°C," *Russian Geology and Geophysics*, vol. 55, no. 10, pp. 1223–1228, 2014.

[12] Y. X. Wang, S. B. Shan, C. Zhang, and P. P. Guo, "Seismic response of tunnel lining structure in a thick expansive soil stratum," *Tunnelling and Underground Space Technology*, vol. 88, pp. 250–259, 2019.

[13] Y. Wang, P. Guo, X. Li, H. Lin, Y. Liu, and H. Yuan, "Behavior of fiber-reinforced and lime-stabilized clayey soil in triaxial tests," *Applied Sciences*, vol. 9, no. 5, p. 900, 2019.

[14] Y. X. Wang, P. P. Guo, H. Lin et al., "Numerical analysis of fiber-reinforced soils based on the equivalent additional stress concept," *International Journal of Geomechanics*, 2019.

[15] T. Meng, Y. Hu, R. Fang, Q. Fu, and W. Yu, "Weakening mechanisms of gypsum interlayers from Yunying salt cavern subjected to a coupled thermo-hydro-chemical environment," *Journal of Natural Gas Science and Engineering*, vol. 30, pp. 77–89, 2016.

[16] Y. Tu, X. Liu, Z. Zhong, and Y. Li, "New criteria for defining slope failure using the strength reduction method," *Engineering Geology*, vol. 212, pp. 63–71, 2016.

[17] D. Krajcinovic and M. A. G. Silva, "Statistical aspects of the continuous damage theory," *International Journal of Solids and Structures*, vol. 18, no. 7, pp. 551–562, 1982.

[18] X. B. Li, S. M. Wang, F. Q. Gong, H. P. Ma, and F. P. Zhong, "Experimental study of damage properties of different ages concrete under multiple impact loads," *Chinese Journal of Rock Mechanics and Engineering*, vol. 31, no. 12, pp. 2464–2472, 2012, in Chinese.